

## IMAGE PROCESSING AND TURING BIFURCATION

**R. Seydel**

*Universität Ulm  
Abteilung Numerik, D-89069 Ulm  
Germany*

الخلاصة :

يمكن تطوير الصور عن طريق معادلة تفاضلية ذات أصول انتشارية. وبصفة عامة فإن الانتشار يُنعم الأحرف والأركان مما يؤدي إلى طمس معلومات مرئية مهمة. يمكن موازنة الأنماط بإدخال حدود تفاعل في المعادلات التفاضلية. هذه الورقة تبيّن كيف نصمم البارامترات في معادلة التفاعل - الانتشار التفاضلية بحيث تصبح أشكالاً معينة مستقرة.

### ABSTRACT

Images can be processed by integrating diffusion-based differential equations. Generally diffusion smoothes edges and corners, thereby blurring important visual information. Patterns can be stabilized by incorporating reaction terms into the differential equations. This paper shows a way how to design the parameters of the reaction-diffusion equation such that specific modes become stable.

## IMAGE PROCESSING AND TURING BIFURCATION

### 1. INTRODUCTION

Traditionally, differential equations were not of primary interest in the field of computer science. Especially, partial differential equations (PDEs) seemed to be invented for classical science areas such as physics. This situation has changed significantly. For a mathematician, it is a pleasure to observe how PDEs have gained the recent attention of researchers in computer vision and image processing. Diffusion-type PDEs have features that match several of the aims of image processing. The basic procedure is as follows: The initial image serves as an initial state for the PDE. Integrating the PDE is then equivalent to processing the initial image. Depending on the type of PDE, the elements in the image may be attenuated or lost, or may be enhanced. Different aims of computerized vision call for specifically designed PDEs.

This paper will show how the two topics, differential equation and bifurcation, can work together in image processing. The first part of the paper presents a brief introduction, and a rudimentary review of PDE-based image processing. One approach is to use the classical linear diffusion equation, which is perfect for noise elimination, and has many advantageous features, but suffers from some limitations. Hence the interest will focus on nonlinear PDEs. Nonlinearity will become the main concern in the second part of the paper, when we describe Turing instability and bifurcation. A *bifurcation analysis* may reveal what kind of structure in the initial image is enhanced. The goal is parameter engineering: We shall attempt to design the PDE in some optimal way. Recent preliminary results based on reaction–diffusion equations will be included.

### 2. DIFFUSION-BASED IMAGE PROCESSING

Let a two-dimensional initial image be described by a real-valued function  $u_0$  defined on a rectangular domain:

$$0 \leq x_1 \leq L_1, \quad 0 \leq x_2 \leq L_2;$$

$(x_1, x_2)$  is the Cartesian location in the image. The values  $u_0(x_1, x_2)$  may represent the grey level function. In case of a colored image we have several of these scalar functions given. The processed values of the initial image  $u_0$  will be denoted:

$$u(x_1, x_2, t), \quad \text{for } t > 0, \quad 0 \leq x_1 \leq L_1, \quad 0 \leq x_2 \leq L_2.$$

The parameter  $t$  (“time”) is the scale parameter, which describes a “distance” between the current version of the processed image, and the initial version  $u_0$  given for  $t = 0$ . Hence we require the initial condition:

$$u(x_1, x_2, 0) = u_0(x_1, x_2) \quad \text{for all } x_1, x_2. \quad (1)$$

This sets the stage for a PDE. Throughout this paper we define  $u(x_1, x_2, t)$  as solution of a PDE

$$\frac{\partial u}{\partial t} = \mathcal{F}(t, x_1, x_2, u, \nabla u, \dots) \quad (2)$$

with initial condition (1), and with appropriate boundary conditions. In Equation (2)  $\frac{\partial u}{\partial t}$  denotes differentiation with respect to  $t$ ;  $\nabla u$  is the gradient operator:

$$\nabla u = \begin{pmatrix} \frac{\partial u}{\partial x_1} \\ \frac{\partial u}{\partial x_2} \end{pmatrix}.$$

The dots in (2) refer to possible higher-order spatial derivatives. The boundary conditions, and the construction of the PDE-model  $\mathcal{F}$  are chosen such that the transformation from  $u_0(\cdot, \cdot)$  to  $u(\cdot, \cdot, t)$  has meaningful features. Along the boundary, Neumann conditions:

$$\mathbf{n}^T \nabla u = 0, \quad (3)$$

are prescribed, where  $\mathbf{n}$  is a vector normal to the boundary;  ${}^t$  means the transposed vector. The Neumann boundary conditions in (3) can be justified by seeing the image  $u_0$  as part of a larger image into which the image  $u_0$  extends.

The main remaining question is how to choose the PDE-model  $\mathcal{F}$ . Here we briefly list a few aims relevant for image processing, namely:

- ( $\alpha$ ) smoothing and damping of perturbations in noise-corrupted images;
- ( $\beta$ ) detecting edges; and
- ( $\gamma$ ) locating corners.

(For an introduction into image processing see, for instance, [1].) We begin with aim ( $\alpha$ ). Later our intention will be to satisfy all of the three aims simultaneously.

It is natural to look into the realm of physics for suitable smoothing mechanisms. The classical diffusion or heat equation:

$$\frac{\partial u}{\partial t} = \operatorname{div} (c \nabla u) = \nabla \cdot (c \nabla u), \quad (4)$$

comes to mind. Whether Equation (4) is linear or nonlinear depends on the function  $c$ . In case of isotropic diffusion ( $c = \text{constant}$ ), Equation (4) is written as:

$$\frac{\partial u}{\partial t} = c \cdot \nabla^2 u. \quad (5)$$

We use the notation  $\nabla^2$  for the Laplacian  $\Delta = \frac{\partial^2}{\partial x_1^2} + \frac{\partial^2}{\partial x_2^2}$ . Applying the *linear diffusion* of Equation (5) with *e.g.*  $c = 1$  dampens the influence of noise or perturbations. The resulting solution  $u(\cdot, \cdot, t)$  of (1), (3), (5) can be also obtained by convolution of  $u_0$  with the Gaussian kernel:

$$G_\sigma := \frac{1}{\sigma} \exp\left(-\frac{x_1^2 + x_2^2}{4\sigma}\right).$$

Note that  $G(x_1, x_2, t) = G_t$  solves the heat Equation (5) for  $c = 1$ . Isotropic Gaussian linear filtering — or linear diffusion — at increasing scales  $t$  not only smooths homogeneous regions corrupted by noise but also gradually smooths relevant image structures such as edge contours. This is demonstrated in Figure 1, where a synthetically generated initial image with  $N \times N$  pixels ( $N = 128$ ) is subjected to the heat equation. The smoothing still allows for edge detection by calculating zero-level curves of  $\nabla^2 u$ ; see [2, 3].

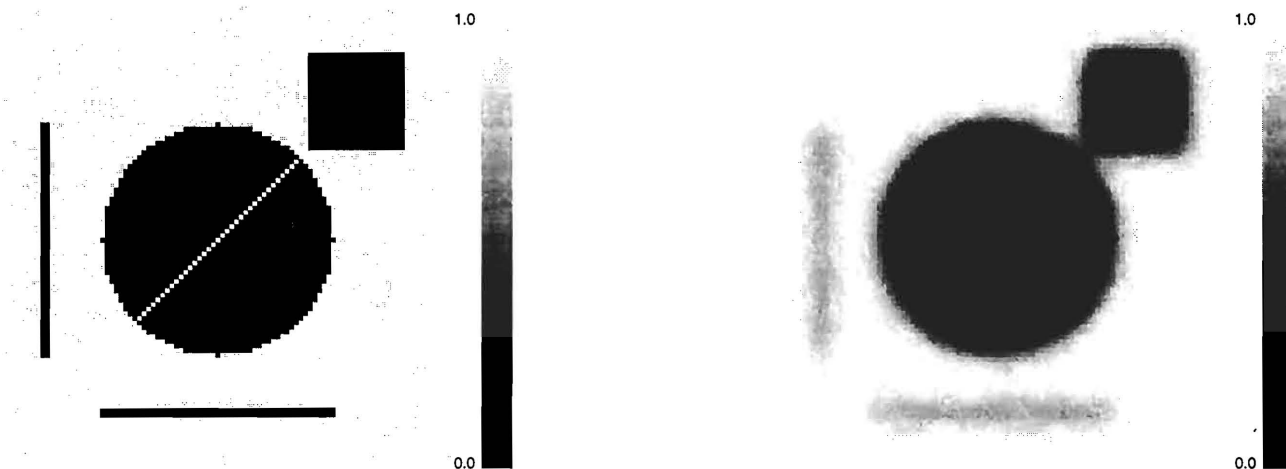


Figure 1. Left: A 10% Noise-Corrupted Test Image  $u_0$ ,  $N = 128$ .  
Right: Processed Version  $u(x_1, x_2, t)$ : Linear Diffusion, Equation (5),  $c = 1$ ,  $t = 4$ .

Malik and Perona [4] have suggested nonlinear diffusion to maintain edges and contrasts. To this end these authors turn diffusion off in case of steep gradients — that is, choose  $c \approx 0$  when  $|\nabla u|$  is large. For example, this aim is achieved by PDE (4) with:

$$c = \exp\left(-\frac{|\nabla u|^2}{K}\right), \text{ with e.g. } K = 100. \tag{6}$$

The features of the Malik and Perona approach and numerical results are described in the literature; see, for instance, [5].

A different approach to smooth the image, and simultaneously preserve edges to some extent, is to allow diffusion only parallel to the edges of contours. This aim can be expressed as a one-dimensional diffusion,

$$\frac{\partial u}{\partial t} = \frac{\partial^2 u}{\partial \xi^2}, \tag{7}$$

where  $\xi$  is the coordinate in the direction of an edge, with angle  $\psi$ , which is orthogonal to the gradient  $\nabla u$ . Some analytical manipulations based on  $u = u(x_1 + \xi \cos \psi, x_2 + \xi \sin \psi)$  show that Equation (7) is equivalent to:

$$\frac{\partial u}{\partial t} = \frac{1}{|\nabla u|^2} (u_{x_1 x_1} u_{x_2}^2 - 2u_{x_1 x_2} u_{x_1} u_{x_2} + u_{x_2 x_2} u_{x_1}^2).$$

This can be expressed by curvature  $\kappa$ ,

$$\kappa = \operatorname{div} \frac{\nabla u}{|\nabla u|} = \frac{u_{x_1 x_1} u_{x_2}^2 - 2u_{x_1 x_2} u_{x_1} u_{x_2} + u_{x_2 x_2} u_{x_1}^2}{(u_{x_1}^2 + u_{x_2}^2)^{\frac{3}{2}}}$$

as

$$\frac{\partial u}{\partial t} = |\nabla u| \kappa = |\nabla u| \operatorname{div} \left( \frac{\nabla u}{|\nabla u|} \right). \tag{8}$$

This equation is called the *mean curvature motion* (MCM) diffusion model.

The features of MCM diffusion, and of related models, have been discussed repeatedly. For an illustration of MCM diffusion see Figure 2. The diffusion causes a level curve to move into the direction of its inner normal. Alvarez *et al.* [6] have shown for the class of PDEs  $u_t = \mathcal{F}(t, x_1, x_2, u, \nabla u, \nabla^2 u)$ , assuming certain reasonable features (causality, invariance, regularity), that  $\mathcal{F}$  must be of the form:

$$\mathcal{F} = |\nabla u| f(\kappa, t), \text{ } f \text{ monotonically growing in } \kappa.$$

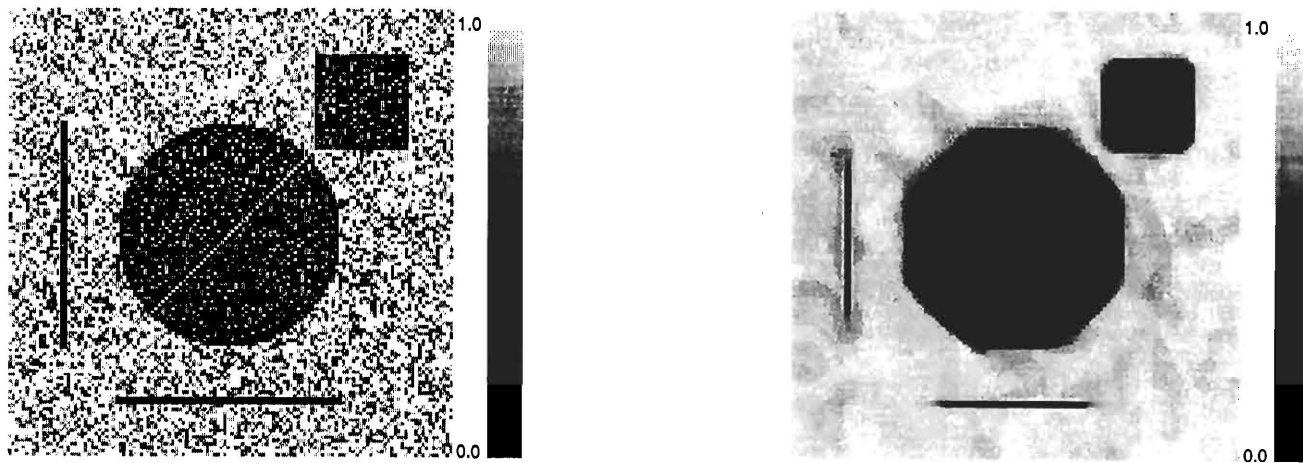


Figure 2. Left: A 50% Noise-Corrupted Test Image,  $N = 128$ .  
Right: Processed Version: MCM, Equation (8),  $u(x_1, x_2, t)$  for  $t = 10$ .

MCM is one prominent example of this class of diffusion equations, with  $f(\kappa, t) = \kappa$ . A smoothing feature of shapes bounded by level curves ( $u = \text{constant}$ ) has been discussed in [7]. Diffusing the derivatives of  $u$  rather than  $u$  has been postulated in [8]. The MCM approach has been modified to control the speed of diffusion, see [9]; for numerical results see also [10].

As the results in Figure 2 indicate, corners are rounded for increasing values of  $t$ , and will be lost for coarse scales. Edges, lines, and corners are not stable under MCM. Ultimately, an amorphous state  $u^s$  of medium grey will take over,

$$\lim_{t \rightarrow \infty} u(x_1, x_2, t) = u^s.$$

In order to stabilize the structure in the image with its corners and edges, a structure-generating “force” will be needed, and/or non-continuous  $u$  must be considered. A natural approach to allow for discontinuous  $u$ , where discontinuities represent edges, is to start from a variational problem instead of a PDE. For related regularization and minimization problems refer to, for example, [11–13]. Whereas the schemes described above utilize a closed-form framework, the biologically motivated FACADE theory [14] segregates mechanisms of contrast and contour processing from those of restoration of invariant features in homogeneous regions. Here, processes of feature diffusion are controlled by activations generated in the parallel contour system. Basically, the diffusion coefficient is reduced at locations of high contrast activity, see [15–17], and the references cited therein. In our framework of studying PDEs, stabilizing activity can be produced by extending the diffusion by some reaction mechanism. Reaction–diffusion as a means to process images has been suggested, for example, in [18, 19]. The remaining part of the paper is devoted to the discussion of stabilizing features of reaction–diffusion.

### 3. TURING INSTABILITY

Reaction–diffusion equations explain pattern formation processes of a wide range of biological and chemical systems [20–24]. Such patterns range from spots or stripes on animal coats to oscillations of concentrations of some chemicals to cardiac arrhythmias. In 1952, Turing laid down a chemical basis of pattern formation, or *morphogenesis*. Turing’s celebrated paper [25] suggests a reaction–diffusion mechanism that explains how patterns may be formed.

In an attempt to describe basic ideas we start from a state that is homogeneous in both space and time. This is the state “no pattern,” or “medium grey”  $u^s$ . For some condition of parameters this state  $u^s$  may be destabilized, and a state is activated that is still stationary with respect to time, but nonhomogeneous in space. This phenomenon of activating a spatial pattern is called the *Turing bifurcation*, or Turing instability, or *diffusive instability*. First, we explain the analytical framework of spatial instability. Later we outline how this mechanism may be used for image processing.

### 4. THE GENERAL ANALYSIS

Using the notations of [26] we consider a system of PDEs of the reaction–diffusion type

$$\frac{\partial \mathbf{y}}{\partial t} = \mathbf{D} \nabla^2 \mathbf{y} + \mathbf{f}(\mathbf{y}, \Lambda), \quad (9)$$

for a vector function  $\mathbf{y}(\mathbf{x}, t)$ . The space coordinate  $\mathbf{x}$  is one-, two-, or three-dimensional. The scalar  $u(\mathbf{x}, t)$  is one component of  $\mathbf{y}$ ; other components of  $\mathbf{y}$  may stand for other channels for processing  $u_0$ . The symbol  $\Lambda$  represents all parameters in the reaction term  $\mathbf{f}$ . Mostly, the matrix  $\mathbf{D}$  is diagonal with the diffusion constants ( $> 0$ ) as entries. Assume  $\mathbf{y}^s$  is a solution both time-invariant and space-invariant,

$$\frac{\partial \mathbf{y}^s}{\partial t} = \mathbf{0}, \quad \nabla \mathbf{y}^s = \mathbf{0}.$$

Consequently,  $\mathbf{y}^s$  satisfies  $\mathbf{f}(\mathbf{y}^s, \Lambda) = \mathbf{0}$ . The state  $\mathbf{y}^s$  stands for a medium grey in image processing. The question is whether  $\mathbf{y}^s$  is stable. To answer this question we briefly outline the standard stability analysis.

Set  $\mathbf{y}(\mathbf{x}, t) = \mathbf{y}^s + \mathbf{d}(\mathbf{x}, t)$ ; this yields:

$$\frac{\partial \mathbf{d}}{\partial t} = \mathbf{D}\nabla^2 \mathbf{d} + \mathbf{f}(\mathbf{y}^s + \mathbf{d}, \Lambda).$$

For  $\mathbf{y}$  close to  $\mathbf{y}^s$  ( $\|\mathbf{d}\|$  small) we truncate,

$$\mathbf{f}(\mathbf{y}^s + \mathbf{d}, \Lambda) = \mathbf{0} + \mathbf{f}_{\mathbf{y}}(\mathbf{y}^s, \Lambda)\mathbf{d} + O(\|\mathbf{d}\|^2),$$

after the linear term to obtain the linearized version of (9):

$$\frac{\partial \mathbf{h}}{\partial t} = \mathbf{D}\nabla^2 \mathbf{h} + \mathbf{f}_{\mathbf{y}}(\mathbf{y}^s, \Lambda)\mathbf{h}. \tag{10}$$

Substituting a separation ansatz  $\mathbf{h}(\mathbf{x}, t) = e^{\mu t}\mathbf{w}(\mathbf{x})$  into (10) leads to the eigenvalue problem:

$$\mu \mathbf{w} = \mathbf{D}\nabla^2 \mathbf{w} + \mathbf{f}_{\mathbf{y}}^s \mathbf{w},$$

which is written:

$$\mathbf{0} = \mathbf{D}\nabla^2 \mathbf{w} + (\mathbf{f}_{\mathbf{y}}^s - \mu \mathbf{I})\mathbf{w}. \tag{11}$$

To study spatial stationary patterns we assume temporal stability — that is, all eigenvalues of the Jacobian  $\mathbf{f}_{\mathbf{y}}^s = \mathbf{f}_{\mathbf{y}}(\mathbf{y}^s, \Lambda)$  have negative real parts. As outlined in Section 2, the diffusion problems we have in mind are best described by zero-flux boundary conditions

$$(\mathbf{n} \cdot \nabla)\mathbf{w} = \mathbf{0}. \tag{12}$$

(In problems with pattern formation, periodic boundary conditions also make sense.) For zero-flux boundary conditions (12) in  $\mathbb{R}^3$ , solutions of (11) consist of eigenfunctions:

$$\mathbf{w}(\mathbf{x}) = \mathbf{a} \cos k_1 x_1 \cos k_2 x_2 \cos k_3 x_3. \tag{13}$$

In the case of one space variable  $x \in \mathbb{R}$ , the resulting ODE-eigenvalue problem for  $0 \leq x \leq L$  is:

$$\mathbf{D}\mathbf{w}'' + (\mathbf{f}_{\mathbf{y}}^s - \mu \mathbf{I})\mathbf{w} = \mathbf{0}, \quad \mathbf{w}'(0) = \mathbf{w}'(L) = \mathbf{0},$$

with eigenfunctions of the type  $\mathbf{w}(x) = \mathbf{w}_k(x) = \mathbf{a} \cos kx$ , and  $k = l\frac{\pi}{L}$ , for  $l = 0, 1, 2, 3, \dots$ . In this context,  $k$  is called the *wave number*. The index  $l$  is the *mode number*.

The following analysis is identical for 1D, 2D, or 3D problems. Because of the applications in visualization we concentrate on the 2D scenario in the rectangle  $0 \leq x_1 \leq L_1, 0 \leq x_2 \leq L_2$ . Accordingly we have wave numbers  $k_1, k_2$ , and mode numbers  $l_1, l_2$ . Substituting (13) into (11), and using the notation  $K^2 := k_1^2 + k_2^2$ , we realize that eigenfunctions  $\mathbf{w}(\mathbf{x})$  and eigenvalues  $\mu$  exist in case:

$$\det(-K^2 \mathbf{D} + \mathbf{f}_{\mathbf{y}}^s - \mu \mathbf{I}) = 0. \tag{14}$$

Note that this equation is invariant of the space dimension. The scalar Equation (14) defines an eigenvalue  $\mu$  for each mode  $(l_1, l_2)$ . In case  $Re(\mu) > 0$  the mode may be activated. The equation  $\mu = 0$  defines a hypersurface  $\mathcal{H}$  in the parameter space that is formed by  $L_1, L_2, \mathbf{D}, \Lambda$ . Each mode  $(l_1, l_2)$  has its own hypersurface,  $\mathcal{H} = \mathcal{H}_{l_1, l_2}$ .

### 5. SPECIAL CASE $n = 2$

In what follows, we simplify the analysis by assuming  $n = 2$  (the smallest dimension of interest). We use the notation

$$\mathbf{A} := \mathbf{f}_{\mathbf{y}}^s = \begin{pmatrix} a_{11} & a_{12} \\ a_{21} & a_{22} \end{pmatrix}, \quad \mathbf{D} = \begin{pmatrix} D_1 & 0 \\ 0 & D_2 \end{pmatrix}, \quad \mathbf{B} := \mathbf{A} - K^2 \mathbf{D}.$$

Then, the vanishing determinant in Equation (14) is simply the quadratic equation

$$\mu^2 - \mu \operatorname{trace} \mathbf{B} + \det \mathbf{B} = 0,$$

with solution

$$\mu = \frac{1}{2} \left( \operatorname{trace} \mathbf{B} \pm \sqrt{(\operatorname{trace} \mathbf{B})^2 - 4 \det \mathbf{B}} \right). \quad (15)$$

Since  $K$  is part of  $\mathbf{B}$ , the eigenvalues  $\mu = \mu_K$  depend on  $k_1, k_2$ , and thus on  $l_1, l_2$ . The Equation (15) is called *dispersion relation*.

After these technical preparations we come back to the question, how the stability of the “no-pattern state”  $\mathbf{y}^s$  may get lost. Note that in the absence of diffusion,  $D_1 = D_2 = 0$ , system (9) reduces to the ODE system  $\dot{\mathbf{y}} = \mathbf{f}(\mathbf{y}, \Lambda)$ . Recall that we assume all eigenvalues of  $\mathbf{A}$  have negative real parts. This criterion for temporal stability in the  $n = 2$  setting is equivalent to the two requirements:

$$\operatorname{trace} \mathbf{A} < 0, \quad \det \mathbf{A} > 0. \quad (16)$$

Assuming (16) means that any loss of stability of the no-pattern state  $\mathbf{y}^s$  must be due to diffusion. The steady state  $\mathbf{y}^s$  is unstable (“Turing unstable”) if for some  $K$

$$\operatorname{Re}(\mu) > 0,$$

for  $\mu$  from (15). The spatial instability can only happen when  $\operatorname{trace} \mathbf{B} > 0$  or  $\det \mathbf{B} < 0$ . Clearly,  $\operatorname{trace} \mathbf{B} > 0$  is not possible because  $\operatorname{trace} \mathbf{B} = \operatorname{trace} \mathbf{A} - K^2(D_1 + D_2)$ ,  $\operatorname{trace} \mathbf{A} < 0$ , and  $D_1 + D_2 > 0$ . Thus, spatial instability of  $\mathbf{y}^s$  within the domain of temporal stability is equivalent to  $\det \mathbf{B} < 0$ , or to:

$$\det \mathbf{A} - K^2(D_1 a_{22} + D_2 a_{11}) + K^4 D_1 D_2 < 0. \quad (17)$$

Clearly,  $\mu \in \mathbb{R}$  for  $\det \mathbf{B} < 0$ . For further analysis, denote the left-hand side of inequality (17) as  $s = s(K^2)$ ,

$$s := \det \mathbf{A} - K^2(D_1 a_{22} + D_2 a_{11}) + K^4 D_1 D_2.$$

Then, for  $n = 2$ , the spatial instability of  $\mathbf{y}^s$ ,  $\mu > 0$ , is equivalent to  $s < 0$ . It remains to discuss the parabola  $s(K^2)$ . This function takes its minimum for:

$$K_{min}^2 = \frac{1}{2} \left( \frac{a_{22}}{D_2} + \frac{a_{11}}{D_1} \right). \quad (18)$$

Equation (18) implies the necessary criterion for spatial instability  $(D_1 a_{22} + D_2 a_{11}) > 0$ . In case  $s(K_{min}^2) < 0$ , there are zeroes  $R_1, R_2$  such that  $s(K^2) < 0$  for the *excitable band*  $R_1 < K^2 < R_2$ . The zeroes are:

$$R_{1,2} = \frac{D_1 a_{22} + D_2 a_{11} \pm \sqrt{(D_1 a_{22} + D_2 a_{11})^2 - 4 D_1 D_2 \det \mathbf{A}}}{2 D_1 D_2}.$$

The threshold values  $K^2 = R_1$ , and  $K^2 = R_2$  correspond to bifurcation values because they are zeroes of the stability-defining function  $s$ . Since the wave numbers  $k_i$  depend on the mode numbers  $l_i$  via  $k_i = l_i \frac{\pi}{L_i}$ , each mode  $(l_1, l_2)$  may have its own bifurcation. For instance, for  $l_2 = 0$ , we obtain from  $l_1^2 \frac{\pi^2}{L_1^2} = R_1$  and  $l_1^2 \frac{\pi^2}{L_1^2} = R_2$  the two relations:

$$l_1^2 \frac{\pi^2}{L_1^2} 2 D_1 D_2 = D_1 a_{22} + D_2 a_{11} \pm \sqrt{(D_1 a_{22} + D_2 a_{11})^2 - 4 D_1 D_2 \det \mathbf{A}}.$$

Such a formula defines a relation among the parameters that fixes a hypersurface in the parameter space where stability of  $\mathbf{y}^s$  can get lost. The parameters include  $L_1, L_2, D_1, D_2$ , and reaction-dependent parameters  $\Lambda$  on

which  $\mathbf{A}$  is based. In particular those modes may be activated with  $K$  close to  $K_{min}$ , see (18). This defines for each pair  $(l_1, l_2)$  a further hypersurface *via* the relation:

$$\pi^2 \left( \frac{l_1^2}{L_1^2} + \frac{l_2^2}{L_2^2} \right) = \frac{1}{2} \left( \frac{a_{22}}{D_2} + \frac{a_{11}}{D_1} \right). \tag{19}$$

### 6. PATTERN FORMATION

For parameters near the hypersurface (19), one or more modes in

$$\sum_{l_1, l_2} \mathbf{a}_K \exp(\mu_K t) \cos \left( \frac{l_1 \pi}{L_1} x_1 \right) \cos \left( \frac{l_2 \pi}{L_2} x_2 \right) \tag{20}$$

have a positive  $\mu$ , and may be activated by perturbations in  $\mathbf{y}^s$ . In case  $L_1, L_2$  are prescribed fixed values we must assume that  $s(K_{min}^2) < 0$  is small enough such that at least one of the discrete values of  $K^2$  is inside the excitable band  $R_1 < K^2 < R_2$ . Note that the exponential growth in (20) for some  $\mu > 0$  has been derived by a linear analysis. Thus its validity is local — the exponential growth is restricted to a short-time period and to a small neighborhood of  $\mathbf{y}^s$ . The activated modes will eventually be dominated and bounded by the nonlinear terms. Ultimately the nonlinearities and initial perturbations will decide which of the modes within the excitable band are activated. The resulting spatial stationary solution  $\mathbf{y}$  is the “pattern.”

In two (or three) spatial dimensions the minimum size that allows some pattern to develop depends on two (or three) directions. The aspect ratio  $L_1/L_2$  of the spatial domain determines the modes of which direction are activated first. On a narrow domain there may be a tendency that several modes in one direction are excited before the first mode in the other direction is activated. For example, for  $L_1 \ll L_2$ , several modes with  $l_1 = 0$  and  $l_2 = 1, 2, \dots$  may be activated *before* the first pattern with  $l_1 \geq 1$  is excited. Nice consequences and interpretations of the predominance of either stripes or spots on animal tails and other animal coats are found in [21, 22].

### 7. NUMERICAL COMPUTATION

For arbitrary  $n$  the homogeneous states  $\mathbf{y}^s$  are the *constant* solutions  $\mathbf{y}(\mathbf{x})$  of the boundary-value problem:

$$\mathbf{0} = \mathbf{D}\nabla^2 \mathbf{y} + \mathbf{f}(\mathbf{y}, \Lambda), \quad (\mathbf{n} \cdot \nabla) \mathbf{y} = \mathbf{0}. \tag{21}$$

The activated non-constant patterns bifurcate from  $\mathbf{y}^s$ . These bifurcations are of pitchfork type (generally without  $\mathbf{Z}_2$ -symmetry). The excitable band is the range of  $K^2$  values such that  $\mu > 0$ . The radii of the excitable band are the same for all dimensions of  $\mathbf{x}$ . Hence we can calculate the hypersurfaces  $\mathcal{H}$  in the parameter space for the relatively simple ODE boundary-value problem with  $x \in \mathbb{R}$ :

$$\mathbf{0} = \mathbf{D}\mathbf{y}'' + \mathbf{f}(\mathbf{y}, \Lambda), \quad \mathbf{y}'(0) = \mathbf{y}'(L) = \mathbf{0}. \tag{22}$$

The hypersurface  $\mathcal{H}$  can be thought of being represented by bifurcation curves in suitable two-dimensional subspaces. The calculation of the bifurcation curves is based on the *branching system*,

$$\begin{pmatrix} \mathbf{D}\mathbf{y}'' + \mathbf{f}(\mathbf{y}, \Lambda) \\ \mathbf{D}\mathbf{h}'' + \mathbf{f}_{\mathbf{y}}(\mathbf{y}, \Lambda)\mathbf{h} \\ p' \end{pmatrix} = \mathbf{0}, \quad \begin{pmatrix} \mathbf{y}'(0) \\ \mathbf{y}'(L) \\ \mathbf{h}'(0) \\ \mathbf{h}'(L) \\ h_l(0) - 1 \end{pmatrix} = \mathbf{0} \tag{23}$$

see [26, 27]. In Equation (23),  $p$  stands for any of the parameters,

$$p \in \Pi := \{L, \mathbf{D}, \Lambda\}.$$

The branching system (23) is solved for various values of a second parameter  $\gamma \in \Pi$  by means of continuation methods; see [26, 27]. This allows to calculate the bifurcation curve, which is cross section of  $\mathcal{H}$  with the  $(p, \gamma)$ -parameter plane. For a multi-parameter problem, several such slices can be calculated to obtain an approximation of  $\mathcal{H}$ . Based on these results the excitable band can be approximated; compare the example of Section 8. The obtained radii bound the excitable bands of the  $\mathbf{x} \in \mathbb{R}^2$ ,  $\mathbf{x} \in \mathbb{R}^3$  situation; no PDEs need be solved for the process of modelling the excitable band. In this way it is possible to efficiently design the parameters that match a specific application.

## 8. EXAMPLE: GIERER–MEINHARDT REACTION

A reaction of the Gierer–Meinhardt [28] type is given by

$$\begin{aligned} u_t &= \nabla^2 u + \frac{u^2}{v} - bu \\ v_t &= D\nabla^2 v + u^2 - v + c. \end{aligned} \quad (24)$$

We study this reaction–diffusion system on an interval  $0 \leq x_i \leq L_i$  for  $i = 1$  ( $x \in \mathbb{R}$ ), or on a rectangle,  $i = 1, 2$  ( $\mathbf{x} \in \mathbb{R}^2$ ). To cut down the dimension of the parameter space  $\Pi$  we choose  $b = 0.5$ ,  $c = 0$  throughout.

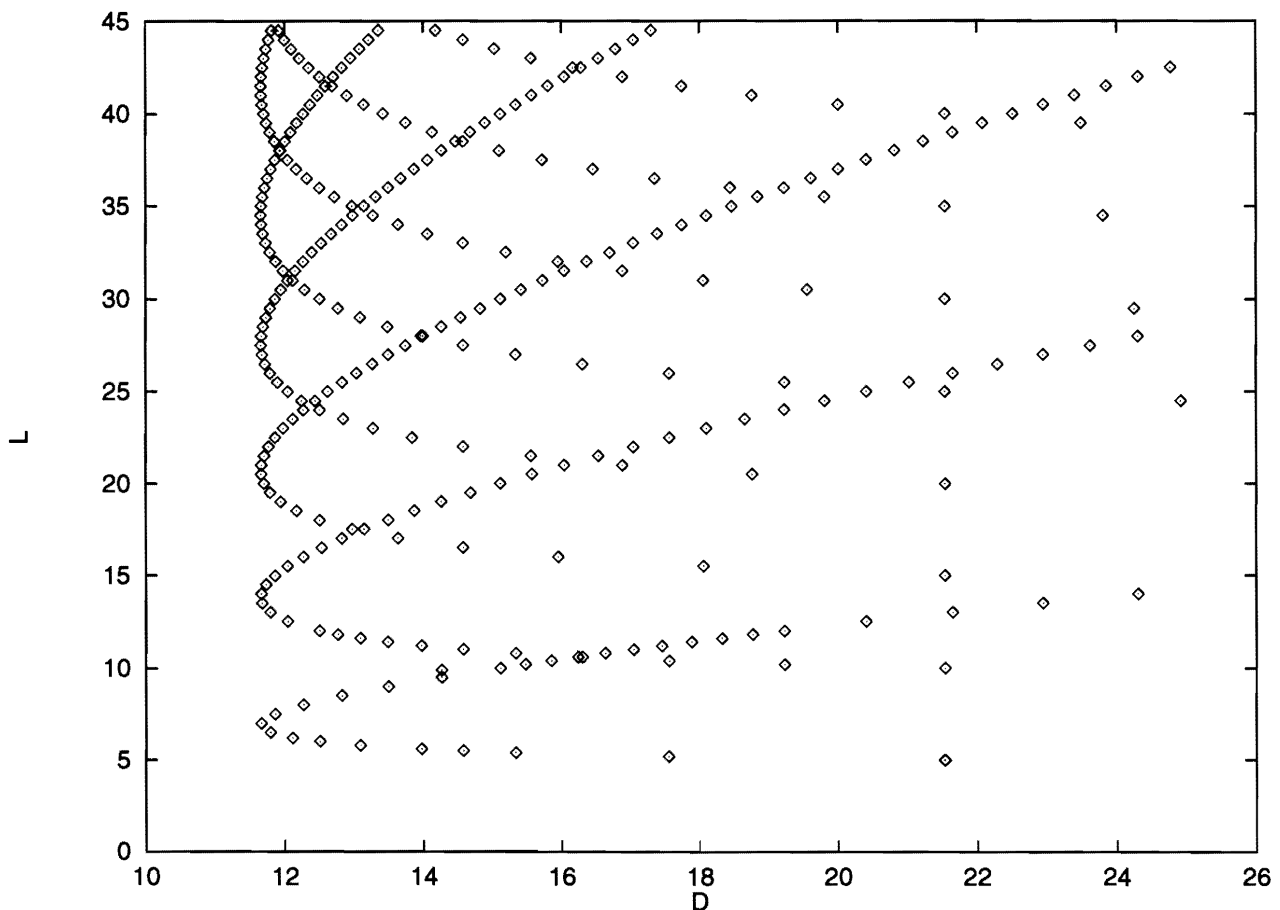


Figure 3. Bifurcation Curves  $\mathcal{H}_l$  in the  $(D, L)$  Plane, for  $l = 1$  (Bottom), ...,  $l = 8$  (Top).

Clearly,  $D_1 = 1$ ,  $D_2 = D$ . For  $x \in \mathbb{R}$ , the situation is analyzed numerically. The hypersurfaces  $\mathcal{H}$  reduce to bifurcation curves in a  $(D, L)$ -plane. These curves have been calculated by solving the branching system that results from the boundary-value problem of the stationary situation  $u_t = v_t = 0$ , see Equation (23), with  $p = D$ ,  $\gamma = L$ . The result is shown in Figure 3 (the calculated points are shown without interpolation). Each of the bifurcation curves corresponds to one mode number  $l$ ; the lowest curve is that of  $l = 1$ . For small  $D$ , and for small values of  $L$  there will be no bifurcation with respect to  $D$ . The length  $L$  must exceed some minimum value in order to let bifurcation or pattern happen.

To see how the results in Figure 3 can be used, assume  $L = 40$ . Clearly, for  $D = 11$  there is no  $\mu > 0$ . For  $D = 12$ , the point  $(D, L) = (12, 40) \in \Pi$  is "outside"  $\mathcal{H}_l$  for  $l = 1, \dots, 5$  and  $l \geq 7$ . But the chosen  $(D, L)$  is "inside"  $\mathcal{H}_6$ . This means that the mode with mode number  $l = 6$  can be activated with the chosen parameter combination. For the 2D-situation with  $L = L_1 = L_2$  this numerically obtained result implies that the modes with

$$l_1^2 + l_2^2 \approx 6^2$$

may be activated. The excitable band is certainly bounded by

$$5^2 < l_1^2 + l_2^2 < 7^2.$$

Interpolation based on the results of Figure 3 allows are to bound the excitable band more accurately. But since the example of Equation (24) is an  $n = 2$  problem, the bounds can be calculated analytically.

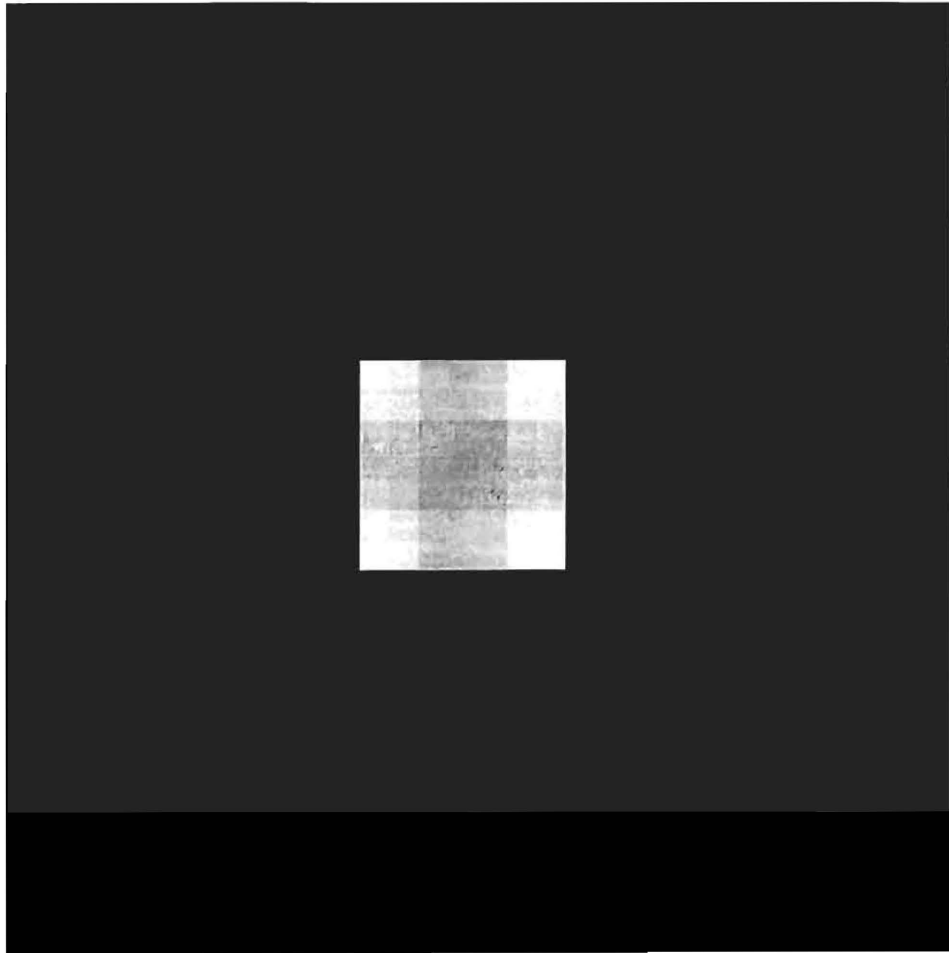


Figure 4. Processing a Square,  $u(t, \mathbf{x})$  for  $t = 5$ ,  $L = 100$ .

## 9. IMAGE PROCESSING

The Gierer–Meinhardt reaction of Equation (24) can be applied for image processing. Assume a square image as input, with light density  $u(\mathbf{x}, 0)$ , for  $0 \leq x_1 \leq L$ ,  $0 \leq x_2 \leq L$ . We are free to assign an arbitrary length  $L$  to the initial image in order to have another free parameter to control the number of active modes. From Section 5, the radii of the excitable band are

$$\frac{L^2}{\pi^2} \sqrt{R_1} \leq l_1^2 + l_2^2 \leq \frac{L^2}{\pi^2} \sqrt{R_2}. \quad (25)$$

For  $c = 0$ , the hypersurface that characterizes  $K_{min}^2$  for the stationary solution  $\mathbf{y}^s = (b^{-1}, b^{-2})$ , with  $a_{11} = b$ ,  $a_{22} = -1$ , is obtained from (18),

$$\frac{\pi^2}{L^2} (l_1^2 + l_2^2) = \frac{1}{2} \left( b - \frac{1}{D} \right).$$

For  $b = 0.5$ ,  $c = 0$ , we choose  $D = 12$ . This choice satisfies the requirements for the existence of an excitable band. The radii are  $R_1 = 1/4$ ,  $R_2 = 1/6$ . In order to obtain a high resolution, many modes should be activated. In view of (25) this calls for large values of  $L$ .

In Figure 4 for  $b = 0.5$ ,  $c = 0$ ,  $D = 12$ ,  $L = 100$ , we show how an initial square  $u(\mathbf{x}, 0)$  has been processed. The 2D differential Equation (24) has been integrated for  $0 < t \leq 5$ , using a discretization of 32 grid points in each direction, with time step  $\Delta t = 0.01$ . The figure shows the state  $u(\mathbf{x}, 5)$ . The stabilization of corners becomes clearly visible.

The analysis of Section 5 allows to reinvestigate the numerical results of Section 8. This reveals for  $L = 40$  from (25) the approximate inequality

$$27 \leq l_1^2 + l_2^2 \leq 40.5.$$

Up to symmetry the mode numbers  $(l_1, l_2) = (4, 4), (3, 5), (2, 5), (1, 6), (2, 6)$  are inside the excitable band. The mode (3,5) is the closest to  $K_{min}^2$ . As another example of applying Section 5, for  $(l_1, l_2) = (1, 0)$  the analysis reveals the bounds  $2\pi \leq L \leq \sqrt{6}\pi$ . Note that these analytical results are shown in Figure 3 as the result of the numerical computation.

## SUMMARY OF THIS PAPER

We have addressed the question of how to design the parameters  $\mathbf{D}, L, \Lambda$  of a reaction–diffusion equation. For each mode number, we are able to approximate the hypersurface  $\mathcal{H}$  in the parameter space that bounds the domain of parameter combinations for which this mode can be activated. Preliminary numerical results suggest that the approach can be used for computerized vision.

## ACKNOWLEDGEMENT

The author thanks Heiko Neumann for fruitful discussions, and for many hints on literature.

## REFERENCES

- [1] R. C. Gonzalez and R. E. Woods, *Digital Image Processing*. Reading: Addison–Wesley, 1992.
- [2] D. Marr and E. Hildreth, “Theory of Edge Detection”, *Proc. Roy. Soc. London Ser.*, **B 207** (1980), pp. 187–217.
- [3] T. Lindeberg, *Scale-Space: A Framework for Handling Image Structures at Multiple Scales*. Report, Stockholm 1996.
- [4] J. Malik and P. Perona, “Scale-Space and Edge Detection Using Anisotropic Diffusion”, *Report No. UCB/CSD 88/483, Computer Science Division EECS, University of California, Berkeley*, 1988.
- [5] B. M. ter Haar Romeny (ed.), *Geometry–Driven Diffusion in Computer Vision*. Dordrecht: Kluwer, 1994.

- [6] L. Alvarez, F. Guichard, P.-L. Lions, and J.-M. Morel, "Axioms and Fundamental Equations of Image Processing", *Arch. Rat. Mech. Anal.*, **123** (1993), pp.199–257.
- [7] B. B. Kimia and K. Siddiqi, "Geometric Heat Equation and Nonlinear Diffusion of Shapes and Images", *Computer Vision and Image Understanding*, **64** (1996), pp.305–322.
- [8] Ge Cong and SongDe Ma, "Nonlinear Diffusion for Early Vision", *Proceedings of the 13th Internl. Conf. Pattern Recognition, Vienna*, 1996.
- [9] L. Alvarez, P.-L. Lions, and J.-M. Morel, "Image Selective Smoothing and Edge Detection by Nonlinear Diffusion, II", *SIAM J. Numer. Anal.*, **29** (1992), pp. 845–866.
- [10] T. Franke, H. Neumann, and R. Seydel, "Anisotropic Diffusion Based on Mean Curvature Motion: a Computational Study", in *Mustererkennung 1996*. ed. B. Jähne *et al.* Berlin: Springer, 1996.
- [11] D. Mumford and J. Shah, "Optimal Approximations by Piecewise Smooth Functions and Associated Variational Problems", *Commun. Pure Appl. Math.*, **42** (1989), pp. 577–685.
- [12] T. Poggio, V. Torre, and C. Koch, "Computational Vision and Regularization Theory", *Nature*, **317** (1985), pp. 314–319.
- [13] C. Schnörr and R. Sprengel, "A Nonlinear Regularization Approach to Early Vision", *Biol. Cybern.*, **72** (1994), pp. 141–149.
- [14] S. Grossberg, "Cortical Dynamics of Three-Dimensional Form, Color, and Brightness Perception", *Perception and Psychophysics*, **41** (1987), pp. 87–158.
- [15] M. Cohen and S. Grossberg, "Neural Dynamics of Brightness Perception: Features, Boundaries, Diffusion, and Resonance", *Perception and Psychophysics*, **36** (1984), pp. 428–456.
- [16] L. Pessoa, E. Mingolla, and H. Neumann, "A Contrast- and Luminance-Driven Multiscale Network Model of Brightness Perception", *Vision Res.*, **35** (1995), pp. 2201–2223.
- [17] H. Neumann, "Mechanisms of Neural Architecture for Visual Contrast and Brightness Perception", *Neural Networks*, **9** (1996), pp. 921–936.
- [18] C. B. Price, P. Wambacq, and A. Oosterlinck, "Applications of Reaction-Diffusion Equations to Image Processing", *Third Int. Conf. on Image Processing and Its Applications*, 1989.
- [19] A. Witkin and M. Kass, "Reaction-Diffusion Textures", *Computer Graphics*, **25** (1991), pp. 299–308.
- [20] H. Meinhardt, *Models of Biological Pattern Formation*. London: Academic Press, 1982.
- [21] L. Edelstein-Keshet, *Mathematical Models in Biology*. New York: McGraw-Hill, 1988.
- [22] J. D. Murray, *Mathematical Biology*. Berlin: Springer, 1989.
- [23] R. Kapral, "Pattern Formation in Chemical Systems", *Physica D*, **86** (1995), pp. 149–157.
- [24] F. W. Schneider and A.F. Münster, *Nichtlineare Dynamik in der Chemie*. Heidelberg: Spektrum Akademischer Verlag, 1996.
- [25] A. M. Turing, "The Chemical Basis of Morphogenesis", *Phil. Trans. Roy. Soc. Lond.*, **B237** (1952), pp. 37–72.
- [26] R. Seydel, "Practical Bifurcation and Stability Analysis", *Springer Interdisciplinary Applied Mathematics Vol. 5*. New York: Springer, 1994.
- [27] R. Seydel, "Nonlinear Computation", *J. of the Franklin Institute*, **8** (1997), pp. 1015–1047.
- [28] A. Gierer and H. Meinhardt, "A Theory of Biological Pattern Formation", *Kybernetik*, **12** (1972), pp. 30–39.

Invited Paper Received 22 March 1997.